Multiple-cascade model for the filling of hollow Ne atoms moving below an Al surface

N. Stolterfoht, A. Arnau,* M. Grether, R. Köhrbrück, and A. Spieler

Hahn-Meitner-Institut, Glienicker Strasse 100, D-14109 Berlin, Federal Republic of Germany

R. Page, A. Saal, J. Thomaschewski, and J. Bleck-Neuhaus

Universität Bremen, Fachbereich 1, D-28359 Bremen, Federal Republic of Germany

Analytic expressions for a multiple-cascade model were derived to study the filling of L and K vacancies of hollow Ne atoms moving in shallow layers of an Al surface. The model requires cross sections for charge transfer into the L shell of the projectile that were determined from molecular-orbital calculations including screening effects of hollow atoms and asymptotic solid-state energies. The analysis accounts for mechanisms of Landau-Zener curve crossing and Fano-Lichten promotion. To describe the transport of the electrons within the solid, absorption and buildup effects were taken into account. The results from the cascade model show good agreement with angular distributions of Ne K Auger electrons recently measured. Attenuation effects were found to produce shifts in the K Auger spectra at varying observation angles. The significant difference previously observed for the mean L-shell occupation numbers during L and K Auger emission is explained by the present model.

PACS number(s): 79.20.Ne, 79.20.Rf, 34.50.Dy

I. INTRODUCTION

The interaction of slow, highly charged ions with surfaces has received a great deal of attention in the past [1–14]. Particularly in recent years, considerable progress has been made in performing experiments with bare and hydrogenlike ions of energies ranging from a few tens of eV to a few tens of keV. In this field, Auger spectroscopy [15–25] has been used extensively among other methods to study the collision dynamics of highly charged ions approaching and entering the surface. Auger transitions are relatively fast so that they serve as a unique "clock" to measure time-dependent phenomena occurring in the 10^{-14}-sec time scale [15]. Hence detailed information about the dynamics of the charge transfer into the slow, highly charged ions has been obtained.

Following the pioneering work by Donets [2], it is now commonly accepted that hollow atoms are produced as the ion approaches the surface. These highly excited atoms have several vacancies in intermediate shells and a corresponding number of electrons in outer shells involving also higher-lying Rydberg states [8,14]. In general, the lifetime of a hollow atom is longer than the time between its formation and its arrival at the surface. Hence, as shown in Fig. 1, the projectile is still hollow when hitting the surface. Then the electrons in higher-lying shells are essentially removed (peeled off) when the projectile enters into the surface [8,10,16]. At the same time, as the projectile merges into the solid, an electronic screening

cloud with a radius equal to a dynamic screening length [26] forms around the ion. The dynamic screening length is generally smaller than the Rydberg orbitals that are peeled off. Thus small hollow atoms (of the second generation) are created within shallow surface layers (inset in Fig. 1).

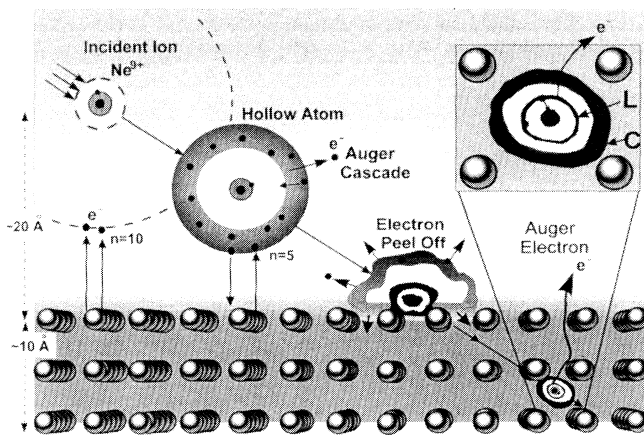Indications for the existence of the hollow atoms

FIG. 1. Formation of hollow atoms above and below the surface. At distances of about 20 Å, the incident Ne^{9+} ion captures several electrons into the Rydberg state $n = \sim 10$. These "large" hollow atoms undergo an Auger cascade reaching lower Rydberg states, e.g., $n = 5$. When the atom hits the surface it is still hollow and the Rydberg electrons are removed (electron peel-off). Simultaneously a dynamic screening cloud (labeled C) is formed around the ion, whereas the L shell (labeled L) stays empty for a certain time. Thus, as shown in the inset, a "small" hollow atom is formed in the solid.

*Permanent address: Departamento de Física de Materiales, Universidad de País Vasco, San Sebastián, Spain.

within the solid have been found in several studies. Briand *et al.* [8], using the method of x-ray spectroscopy, provided clear evidence that the L shell of Ar is still mostly empty when radiative K-shell transitions occur within the solid. In contrast to x-ray spectroscopy. Auger electron spectroscopy has been performed under the assumption of above-surface emission for quite some years [4,5,18] until Meyer *et al.* [15] and Burgdörfer, Lerner, and Meyer [16] concluded from detailed model calculations that the majority of the observed Auger electrons originate from below the surface. Nevertheless, much attention continued to be devoted to small structures in the Auger spectra considered to be due to above-surface emission [15,16,18,20]. These structures are still debated [22,24].

More recently, the Auger peak profiles originating from below surface emission have been examined in detail. Initial comparisons of experimental Ne Auger spectra with extensive atomic-structure calculations have been performed by Köhrbrück *et al.* [17] and Schippers *et al.* [19], showing two essential features: (i) Several electrons are missing in the L shell during K Auger transitions and (ii) the missing electrons are located in the M shell so that the whole atomic complex is neutral. Thus, today, it has become common practice in calculations of Auger transitions near the surface that electrons missing in inner or valence shells are filled into the next-higher-lying orbital [18,22,25]. Recently, it was recognized that this "filling-up" procedure models the dynamic screening cloud formed around the ion in the solid [22,24]. Thus, when a first-row ion such as Ne^{9+} enters a solid, a dynamic screening cloud of the size of the M shell is formed, whereas its L shell remains empty for a finite time. In other words, a hollow Ne atom is created in the solid.

The characteristic lifetime needed for the filling of the hollow atom is still a matter of controversy. The filling mechanism is due to a cascade process where the transfer of electrons into the L shell is followed by a K Auger transition. This picture suggests the use of a two-step model for the description of light ions [15,20,22]. As details of the filling mechanism are missing in such a simple approach, the two-step model has been applied with only moderate success. Hence it is advantageous to use a multiple-cascade model, which has already been considered in the early x-ray spectroscopy work by Briand *et al.* [8]. Detailed cascade models have previously been utilized to describe the relaxation of hollow atoms above and at the surface under grazing incident conditions [10,16,27]. Recently, for the case of Auger emission from highly charged projectiles moving inside the solid, a multistep cascade model has been worked out by Page *et al.* [28] revealing detailed information about the filling of hollow Ne atoms.

In the present work, the multistep cascade model of Page *et al.* [28] was modified in several aspects. First, the model was simplified to achieve analytic expressions for the Auger electron emission. This was primarily done by neglecting the scattering of the incident ions by assuming a straight-line trajectory for the projectile. On the other hand, for the transport of the Auger electrons,

absorption and buildup effects in the solid were incorporated by using simple exponential attenuation laws. The use of exponential functions allowed for the preservation of analytic solutions of the integrated Auger intensities. Hence the present approach will sometimes be referred to as the *analytic cascade model.* Furthermore, besides the treatment of the K Auger decay, the emission of L Auger electrons was explicitly taken into account.

In view of the previous work by Meyer *et al.* [15] and Köhrbrück *et al.* [22], we disregard above-surface emission of Auger electrons. The main emphasis is given to the determination of cross sections for collisional L-shell filling of the projectile moving within the solid. Such cross sections have previously been treated as unknown model parameters that were adjusted in fitting procedures [15,22,28]. Here the cross sections for charge exchange from an Al target into a hollow Ne atom moving in the solid were calculated. Couplings were considered between molecular orbitals transiently formed during the collision. Both Landau-Zener transitions [29] and Fano-Lichten promotion mechanisms [30] were treated in the analysis. The Landau-Zener treatment is similar to that previously used by Schippers *et al.* [19]. In the present study, however, an attempt is made to account for the properties of the hollow atoms in the derivation of the charge-exchange cross sections. It should be noted that preliminary results of the present analysis have recently been reported [31].

The present work is structured as follows. In Sec. II the analytic cascade model is outlined. In Sec. III molecular-orbital (MO) diagrams involving hollow atoms are given. In Sec. IV the corresponding cross sections for the L-shell filling are evaluated by means of the MO data. In Sec. V the analytic cascade model is applied to analyze previous experimental data. Since the emphasis is focused on the evaluation of the L-shell filling cross sections, only a few applications of the present cascade model are given. Nevertheless, it will be shown that the present model is capable of reproducing various aspects concerning the filling of hollow atoms below the surface.

II. MULTIPLE-CASCADE MODEL

The dynamics of the L- and the K-shell filling are determined by expressions that are similar to those known from radioactive decay of nuclei. The different mechanisms are shown schematically in Fig. 2. The fillings of the projectile L shell take place via L Auger transitions and collisional charge transfer governed by both the L Auger rate Γ_{Ln} and the capture rate Γ^c_{Ln}, respectively, where n is the number of electrons already occupying the L shell. After two electrons have been transferred into the L shell, one may observe K Auger transitions associated with the K Auger rate Γ_{Kn}.

As pointed out by Page *et al.* [28], the time-dependent number of atoms $N_n(t)$ with one vacancy in the K shell and n electrons in the L shell is obtained by solving the rate equations

$$\frac{dN_n}{dt} = \Gamma^f_{Ln-1}N_{n-1} - S_n N_n \ , \tag{1}$$

where the L-shell filling rate $\Gamma^f_{Ln} = \Gamma^c_{Ln} + \Gamma_{Ln}$ and the sum rate $S_n = \Gamma^f_{Ln} + \Gamma_{Kn}$ are obtained from the individual rates summarized in Table I. The rate equation can be solved analytically by means of linear combinations of exponential functions as shown in various textbooks (e.g., [32]):

$$N_n(t) = \prod_{i=0}^{n-1} \Gamma^f_{Li} \sum_{j=0}^{n} \frac{e^{-S_j t}}{\prod\limits_{i\,(\neq j)=0}^{n} (S_i - S_j)} . \tag{2}$$

It should be noted that the cascade process starts at $t=0$ without any electron in the L shell of the hollow projectile.

As mentioned above, for $n \geq 2$ the ensemble of atoms $N_n(t)$ undergoes K Auger transitions with the rate Γ_{Kn}. The number of K Auger electrons ejected per unit time is obtained as

$$I_{Kn}(t) = N_n(t)\Gamma_{Kn} . \tag{3}$$

Since the Auger electrons are ejected within the solid, the flux of the K Auger electrons on their way out to the surface is reduced primarily by inelastic collisions. We assume an exponential attenuation law

$$a_K(t) = e^{-\Gamma^a_K t} , \tag{4}$$

where Γ^a_K is the attenuation rate (Table I). This time-dependent attenuation law follows directly from the

TABLE I. Summary of the rates used in the analysis; see the text for details. The data apply for the number n of electrons in the L shell of Ne moving in solid Al.

Type of rate	L shell	K shell
Capture	$\Gamma^C_{Ln} = \sigma_{Ln} n_c v_p$ $n_c = 0.009$ a.u.	
Auger	$\Gamma_{Ln} = (8-n)\Gamma_L$ $\Gamma_L = 0.67 \times 10^{-3}$ a.u.	$\Gamma_{Kn} = (n-1.3)\Gamma_K$ $\Gamma_K = 1.4 \times 10^{-3}$ a.u.
Attenuation	$\Gamma^a_L = v_l / \lambda^a_L$ $\lambda^a_L = 8$ a.u.	$\Gamma^a_K = v_l / \lambda^a_K$ $\lambda^a_K = 30$ a.u.
Attenuation for buildup	$\Gamma^b_L = v_l / \lambda^b_L$ $\lambda^b_L = 17$ a.u.	$\Gamma^b_K = v_l / \lambda^b_K$ $\lambda^b_K = 80$ a.u.

well-known expression $a_K(l) = e^{-l/\lambda^a_K}$, where l is the travel distance of the electrons in the solid and λ^a_K is the corresponding attenuation length. Within the present approximation of a projectile moving with a constant velocity v_p on a straight-line trajectory, the distance l is proportional to the time t. The proportionality constant is the "velocity" v_l which in turn can be used to express the attenuation rate as $\Gamma^a_K = v_l / \lambda^a_K$ (Table I). From geometrical considerations [22] it follows that $v_l = v_\perp / \sin\alpha$, where $v_\perp = v_p \sin\psi$ is the velocity component perpendicular to the surface plane, α is the electron observation angle relative to that plane, and ψ is the incident angle of the projectile.

By time integrating one obtains the *attenuated intensity* of the Auger electrons in the elastic channel

$$Y^a_{Kn} = \int_0^\infty a_K(t) I_{Kn}(t) dt , \tag{5}$$

which may be evaluated analytically giving rise to the relatively simple expression

$$Y^a_{Kn} = \Gamma_{Kn} \frac{\prod\limits_{i=0}^{n-1} \Gamma^f_{Li}}{\prod\limits_{i=0}^{n} \tilde{S}^a_{Ki}} , \tag{6}$$

where $\tilde{S}^a_{Ki} = S_i + \Gamma^a_K$ is the sum rate modified by attenuation. It is noted that Limburg *et al.* [33] have derived a similar expression that applies for the case of vanishing attenuation effects on the electron traveling in the solid.

The Auger electrons, lost by attenuation, are primarily scattered into the inelastic channel where the creation of Auger intensity is governed by the *buildup function*

$$b_K(t) = (1 - e^{-\Gamma^a_K t}) e^{-\Gamma^b_K t} . \tag{7}$$

The first term describes the buildup in the inelastic channel and the second term governs its absorption, which in turn is determined by the attenuation rate Γ^b_K (Table I). Similarly to the primary channel, the flux in the inelastic channel is integrated to obtain the *buildup intensity*

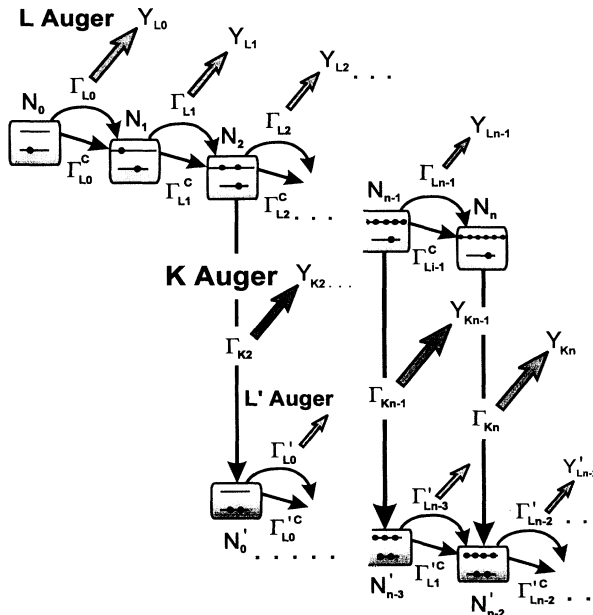$$Y^b_{Kn} = \int_0^\infty b_K(t) I_{Kn}(t) dt , \tag{8}$$

FIG. 2. Diagram for multiple cascade processes in hollow atoms moving below a surface. The label n specifies the number of L-shell electrons. The quantities Γ_{Ln} and Γ_{Kn} are L and K Auger rates. The quantities Γ^c_{Ln} are rates for collisional transfer of an electron into the L shell. The arrows indicate the intensity of the ejected L and K Auger electrons.

which may again be solved analytically. The result is obtained as the difference of two terms, each one analogous to that given in Eq. (6):

$$Y_{Kn}^b = \Gamma_{Kn} \left[\frac{\prod_{i=0}^{n-1} \Gamma_{Li}^f}{\prod_{i=0}^{n} \tilde{S}_{Ki}^b} - \frac{\prod_{i=0}^{n-1} \Gamma_{Li}^f}{\prod_{i=0}^{n} \tilde{S}_{Ki}^{ab}} \right] , \quad (9)$$

where the sum rate $\tilde{S}_{Ki}^a$ in Eq. (6) is replaced by $\tilde{S}_{Ki}^b = S_i + \Gamma_K^b$ and $\tilde{S}_{Ki}^{ab} = S_i + \Gamma_K^a + \Gamma_K^b$, respectively. The Auger electrons are usually measured within a wide range of energies, covering most of the inelastic energy spectrum, so that the quantity observed in the experiment is the *transported intensity*

$$Y_{Kn} = Y_{Kn}^a + Y_{Kn}^b . \quad (10)$$

For the analysis of hollow atoms it is useful to evaluate mean values from the foregoing analytic expressions. As the attenuation modifies the electron intensities, we shall distinguish between the *apparent* mean values and the *actual* mean values depending on whether the attenuation effects do or do not play a significant role. For instance, we define the *apparent mean depth* $\langle \tilde{z} \rangle_{Kn}$ for the emission of K Auger electrons, attributed to the number n of L-shell electrons, taking into account the attenuations in the elastic and inelastic channels

$$\langle \tilde{z} \rangle_{Kn} = \frac{v_\perp}{Y_{Kn}} \int t[a_K(t) + b_K(t)] I_{Kn}(t) dt , \quad (11)$$

where $v_\perp$ is again the perpendicular component of the projectile velocity (assumed to be constant). Similarly, we define *the actual mean depth* $\langle z \rangle_{Kn}$, which would be observed if the attenuation of the Auger electrons were negligible, i.e., $a_K + b_K = 1$ in Eq. (11). Analogously, the mean depths $\langle \tilde{z} \rangle_K$ and $\langle z \rangle_K$ are obtained after summing over the number of L-shell electrons.

Furthermore, time integration yields the *apparent mean number* $\langle \tilde{n} \rangle_K$ of L-shell electrons during the K Auger decay

$$\langle \tilde{n} \rangle_K = \frac{1}{Y_K} \sum_{n=2}^{8} n Y_{Kn} , \quad (12)$$

where $Y_K = \sum_{n=2}^{8} Y_{Kn}$ is the total K Auger intensity. Again, the *actual mean number* $\langle n \rangle_K$ is obtained for negligible attenuation $\Gamma_K^a = 0$. Furthermore, one may consider the particular mean numbers $\langle \tilde{n} \rangle_K^a$ and $\langle \tilde{n} \rangle_K^b$, due to the elastic and inelastic channels, where Y_{Kn} is replaced by Y_{Kn}^a and Y_{Kn}^b, respectively. It should be noted that, generally, the apparent mean number $\langle \tilde{n} \rangle_K^a$ is most relevant for the experiments, as the elastic intensities are responsible for the pronounced Auger peak. For Al, however, the inelastic intensities also contribute noticeably to the Auger peak [34].

Finally, it is pointed out that the present expressions apply also for L Auger emission when the label K is replaced by L. It should be noted, however, that the L Auger emission implies another decay channel that is active after the K Auger transition has occurred. The K

Auger transition creates two more L-shell vacancies so that an increased number of L Auger electrons is produced. The corresponding L-shell Auger transitions are referred to as the primed Auger rate Γ'_{Ln} (Fig. 2). In the present work, these (primed) L Auger electrons were not taken into account. We were not sure whether these Auger electrons are observed in the experiments, as the corresponding Auger energies are shifted to lower energies [35] and hence they may be lost in the continuous background. The search for these L Auger electrons will be performed in a forthcoming study.

The quantities Γ_L and Γ_K (Table I) are proportionality constants in the evaluation of the individual L and K Auger rates, respectively. The K Auger rates Γ_{Kn} were determined empirically [28] by fitting theoretical Ne data from the literature [36]. The results of the fit are shown in Fig. 3, yielding the empirical function $\Gamma_{Kn} = (n - 1.3)\Gamma_K$ for $n \geq 2$, where the proportionality constant is found to be $\Gamma_K = 1.4 \times 10^{-3}$. Since we could not find adequate L-shell Auger rates for different L-shell occupation numbers, we assumed that the L Auger rate Γ_{Ln} is proportional to the number of vacancies $\bar{n} = 8 - n$ in the L shell (Table I). The proportionality constant Γ_L was extrapolated from $\bar{n} = 1$ data given in the compilation by Krause [37]. Hence we found that $\Gamma_L \approx \Gamma_K / 2$ (Table I). This result appears reasonable since we would not expect large differences between K and L Auger rates.

The quantities λ_L^a and λ_K^a are the attenuation lengths for L- and K-shell electrons, respectively, and λ_L^b and λ_K^b are the corresponding attenuation lengths for buildup (Table I). They were determined by fitting the sum of Eqs. (4) and (7) to results from Monte Carlo calculations by Page *et al.* [28]. The fitted attenuation lengths are consistent with the calculations by Nunez, Echenique, and Ritchie [38]. We recall that the definition of the attenuation rates is based on the constant velocity $v_l = l / t$
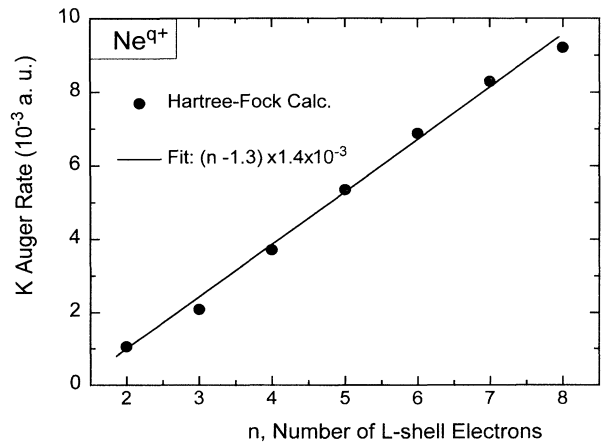

FIG. 3. Neon K Auger rates as a function of the number n of L-shell electrons. To obtain the present results, previous Auger rates (points) by Chen and Craseman [36] are averaged under the assumption of a statistical population of the associated multiplet terms. They are fitted by the empirical expression $(n - 1.3)1.4 \times 10^{-3}$.

(Table I), which involves the approximation of a straight-line trajectory of the projectile. It should be added that we implemented the refraction of the Auger electrons near the surface due to its work function as discussed in more detail by Page et al. [28]. For the present K Auger intensities the refraction effects were found to be small, whereas they are essential for the L Auger intensities.

The unknown quantities of the multiple-cascade model are the capture rates Γ^c_{Ln}, which in turn are determined by the cross sections σ_{Ln} for collisional filling of the projectile L shell. As shown in Table I, the capture rate Γ^c_{Li} is a product of the L-shell filling cross section σ_{Ln}, the spatial density n_c of the collision centers, and the projectile velocity v_p [22]. These cross sections are evaluated by analyzing transitions between MO's that are formed as the hollow projectile atom approaches a target atom in the solid. The evaluation of the MO's will be outlined in the following section.

III. MOLECULAR-ORBITAL DIAGRAMS

The construction of the MO's has recently been described by Arnau et al. [39]. As additional examples for MO diagrams are presented, a few details of the analysis shall be given here. The MO calculations are based on matrix elements that have been evaluated previously within a screened hydrogenic model (SHM) by Stolterfoht [40]. They are given as a function of the internuclear distance R (in atomic units):

$$H^N_{ii} = \varepsilon^0_i - \frac{1 - e^{-d\alpha_i R}}{R} Q_M(R) , \tag{13a}$$

$$H^N_{ij} = -\frac{3}{2} \frac{1 - P(d'\alpha_{ij}R)e^{-d'\alpha_{ij}R}}{\tilde{\alpha}_{ij}R^2} Q_M(R) , \tag{13b}$$

$$H_{ij} = k\tilde{\alpha}^2_{ij}e^{-c\alpha_{ij}R} , \tag{13c}$$

where i and j label the L-shell orbitals $2s$ and $2p$ centered at the collision partners labeled N and M. Equation (13a) represents the diagonal matrix elements, whereas Eqs. (13b) and (13c) describe the nondiagonal matrix elements of orbitals located at one center and two centers, respectively. In Eq. (13b) the polynomial $P(x) = \sum^4_{\nu=0} x^\nu/\nu!$.

The model matrix elements contain dimensionless parameters that are treated as constants after they have been adjusted to fit molecular orbitals evaluated independently by means of a Hartree-Fock code [40]. For the present case, the results for the constants are $c = 0.86$, $d = 0.5$, $d' = 1.5$, and $k = 3.6$. The variable quantities of the SHM matrix elements are the velocity parameters $\alpha_i = |2\varepsilon^0_i|^{1/2}$ deduced from the corresponding binding energies ε^0_i. These quantities were utilized to determine the mean values $\alpha_{ij} = (\alpha_i + \alpha_j)/2$ and $\tilde{\alpha}_{ij} = (\alpha_i\alpha_j)^{1/2}$. Similarly, the mean value $\alpha_M = (\alpha_{2s} + \alpha_{2p})/2$ was deduced from the $2s$ and $2p$ orbitals located at center M.

Originally, for ground-state atoms, a simple exponential screening was used:

$$Q_M(R) = Z^{eff}_M \exp(-\alpha_0 R) , \tag{14}$$

where $Z^{eff}_M = 2\alpha_M$ is the effective nuclear charge of center M and $\alpha_0 = 0.86$ a.u. is an outer-shell screening parameter [40]. In the present work, the screening function was modified to model the features of hollow projectile atoms. Furthermore, solid-state effects were taken into account. Total energies of separated atoms in a solid were obtained using density-functional theory as applied to the problem of a static impurity in jellium and specifying a certain set of occupation numbers for the bound levels of the ion that correspond to each particular electronic configuration [41,42]. Then, the orbital energies for the multicharged Ne ion (with one K-shell vacancy) in Al were calculated from total-energy differences. More details are given in the work by Arnau et al. [39].

The model matrix elements from Eqs. (13a)–(13c) were used to evaluate the corresponding MO energies by means of numerical diagonalization [43]. The results for σ orbitals are given in Figs. 4(a)–4(f), which refer to Ne with an increasing number of L-shell electrons. Asymptotically, at large internuclear distances, the MO's correlate to the $2s$ and $2p$ level of Ne and Al. It is seen [in particular from Fig. 4(a)] that the $4f\sigma$ orbital, correlated to the Al $2p$ level, decreases strongly in energy with decreasing distance. This orbital demotion occurs before the characteristic $4f\sigma$ promotion predicted by the Fano-Lichten model [30]. For the present application it is noted that vacancies rather than electrons are promoted.

The present orbital demotion can be considered as a specific effect of the hollow atom that contains several va-
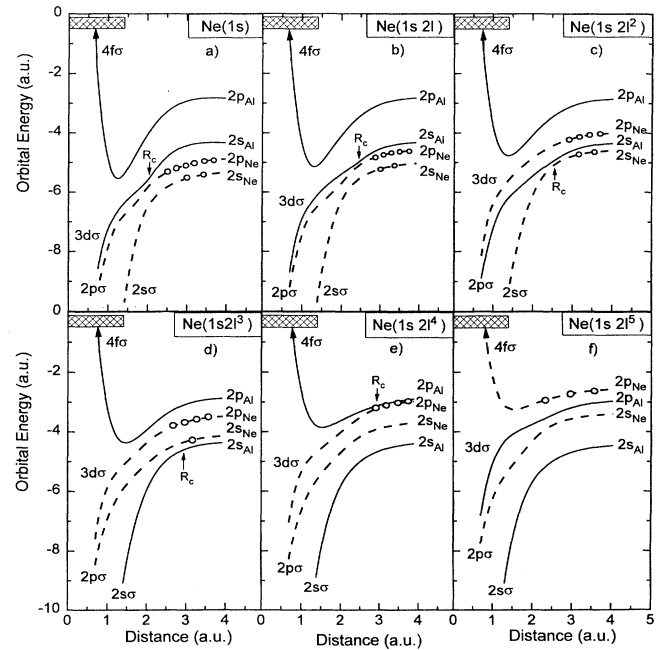
FIG. 4. Molecular-orbital energies for the hollow Ne plus Al system evaluated by diagonalization of model matrix elements [40]. (a)–(f) Data for 0–5 electrons in the Ne L shell, respectively. The arrows labeled R_c indicate crossings of the underlying diabatic potential curves.

cancies in the L shell and hence strongly affects the collision partner Al at intermediate distances. Inspecting the diagrams from Figs. 4(f) to 4(a) it is seen that the orbital demotion becomes more important for an increasing number of L-shell vacancies. The strong orbital demotion also causes the approach of the $3d\sigma$ MO and the $2p\sigma$ MO so that an avoided crossing appears at about 2.2 a.u., indicated by an arrow labeled R_c in Fig. 4(a). Here couplings between the MO's occur, transferring electrons into the empty L shell of Ne. A similar crossing occurs between the $3d\sigma$ and the $2p\sigma$ MO's correlated to the Al $2s$ and the Ne $2p$ levels, respectively [see the arrow in Fig. 4(b)].

As the number of L-shell electrons further increases to $n \geq 5$, the $2p$- level of Ne is shifted beyond the Al $2p$ level. Then, the Ne $2p$ level correlates to the $4f\sigma$ MO so that the remaining vacancies are likely to be promoted into the conduction band of Al [Fig. 4(f)]. The probabilities for the electron transfer will be evaluated in the next section.

IV. CROSS SECTIONS FOR L-SHELL FILLING

The model matrix elements [40] and the associated MO energies were used to calculate probabilities for the transfer of electrons into the L shell of the hollow Ne projectile. Essentially, two models were used in the analysis. The Landau-Zener model [29] was utilized at curve crossings [Figs. 4(a)–4(e)], whereas the Fano-Lichten model [30] was applied in cases of orbital promotion [Fig. 4(f)]. The Fano-Lichten model was applied here to the case of hollow atoms colliding with an atom in the solid.

Before curve crossings and electron promotion are considered, the populations of the associated molecular orbitals are evaluated. Again, vacancies rather than electrons are considered in the analysis. It is noted for decreasing internuclear distance that the $2s$ levels develop into σ orbitals whereas the $2p$ levels split into σ and π orbitals. It has previously been shown that the π orbitals are less important for vacancy exchange between closely lying L-shell levels [40]. Hence the attention is focused on the σ orbitals (Fig. 4) whose vacancy occupation is determined by statistical rules. As the σ orbital implies two spin states, it may contain up to two vacancies. Vacancies present in the $2s$ level are all transferred into the corresponding σ orbital. The transfer probabilities for one or two vacancies from the $2p$ level into the σ orbital are governed by well-known statistical rules, i.e.,

$$P_\sigma^{(1)} = 2p_\sigma(1-p_\sigma), \quad P_\sigma^{(2)} = p_\sigma^2 , \tag{15}$$

where $p_\sigma = \bar{n}_{2p}/6$ is the corresponding σ transfer probability per spin state and $\bar{n}_{2p}$ is the number of $2p$ vacancies. For instance, an empty L shell implies $\bar{n}_{2p} = 6$ and hence it follows that $P_\sigma^{(1)} = 0$ and $P_\sigma^{(2)} = 1$. For $\bar{n}_{2p} < 6$ one obtains $P_\sigma^{(1)} > 0$ and $P_\sigma^{(2)} < 1$.

When the internuclear distance decreases further, adjacent orbitals may interact. Transitions between these orbitals are described by the Landau-Zener model, which applies for a crossing of the diabatic potential curves at the internuclear distance R_c (crossing radius), assuming a

constant coupling matrix element within the coupling region. The probability for transitions between the adiabatic states is given by [29]

$$p_{Ln} = \exp\left[-\frac{2\pi |H_{ij}(R_c)|^2}{v_R F_{ij}(R_c)} \right] , \tag{16}$$

where $H_{ij}(R_c)$ is the nondiagonal matrix element from Eq. (13c), $F_{ij}(R_c) = d(H_{ii} - H_{jj})/dR$ is the measure for the inclination of the diabatic potential curves at the crossing radius R_c with H_{ii} and H_{jj} being taken from Eq. (13a), and v_R is the radial velocity of the collision partners. Following the methods in Ref. [40] we have set approximately $v_R \approx v_p/\sqrt{2}$, where v_p is again the projectile velocity.

As the coupling region is passed twice during the collision, different cases of vacancy transfer are evaluated by means of statistical laws. The probabilities for the transfer of one and two vacancies are given by

$$P_{Ln}^{(1)} = P_\sigma^{(1)} 2p_{Ln}(1-p_{Ln}) + P_\sigma^{(2)} 4[p_{Ln}(1-p_{Ln})^3$$
$$+ p_{Ln}^3(1-p_{Ln})] , \tag{17}$$

$$P_{Ln}^{(2)} = P_\sigma^{(2)} 4p_{Ln}^2(1-p_{Ln})^2 , \tag{18}$$

where the first and the second terms on the right-hand side of Eq. (17) originate from the occupation of the σ orbital by one and two vacancies, respectively.

It is seen from Fig. 4(f) that the $4f\sigma$ orbital is strongly promoted at an internuclear distance of about 1 a.u. In this case, vacancies are transferred to higher-lying orbitals or the conduction band of the Al solid. As shown in various studies [30,44,45], the Fano-Lichten promotion mechanism is so effective that one expects the removal of *two* vacancies from the $4f\sigma$ orbital once the impact parameter is equal to or smaller than a certain threshold R_c. Hence, for internuclear distances $R_c \leq 1$ a.u. [Fig. 4(f)], we set the probabilities to its maximum value, i.e., $P_{Ln}^{(1)} = P_{Ln}^{(2)} = 1$.

Finally, the corresponding transfer cross sections, i.e., for the filling of one and two electrons into the L shell of the projectile, are obtained in the following "geometric" approximation [45]:

$$\sigma_{Ln}^{(i)} = P_{Ln}^{(i)} \pi R_c^2 , \tag{19}$$

where the label i stands for the transfer of one and two vacancies. As before, R_c is the associated coupling radius. The results of the cross-section calculations are shown in Fig. 5, where data for $n \leq 4$ are obtained by means of the Landau-Zener model and for $n \geq 5$ they are evaluated on the basis of the Fano-Lichten promotion model. In the case $n = 3$ we also used models by Demkov [46] and Nikitin [47]. Moreover, these models were applied to estimate (small) contributions from the coupling of the π orbitals.

The foregoing analysis has shown that up to two vacancies may be transferred in a single binary collision between the projectile and the solid target atom. The probability for double vacancy transfer is small however, so its influence on the L-shell cascade is not expected to be
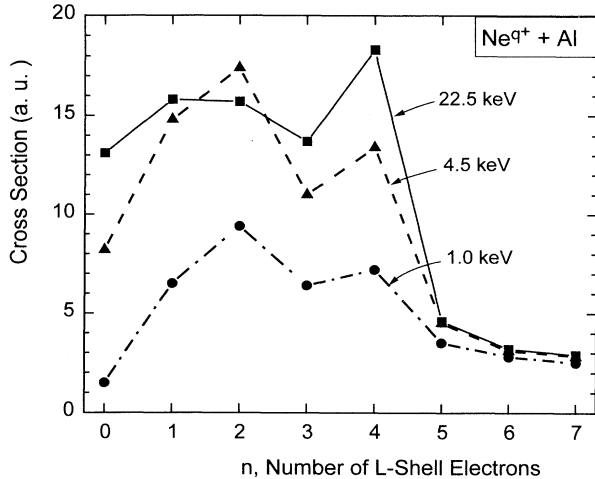
FIG. 5. Cross sections for charge transfer into the L shell of hollow Ne. Projectile energies are 1.0, 4.5, and 22.5 keV as indicated. The results for $0 \leq n \leq 4$ are obtained from the Landau-Zener formula and for $n \geq 5$ from the Fano-Lichten model. To convert the cross sections to cgs units multiply by 2.8×10^{-17} cm^2/a.u.

significant. It should be realized that the inclusion of the double vacancy transfer would exclude an analytical solution of the rate equations. To retain the simplicity of the present analysis, the double vacancy transfer was taken into account in an approximate manner. The cross sections for double vacancy transfer were multiplied by a factor of 2 and added to the corresponding cross section for single vacancy transfer. This procedure appears to be reasonable in view of the uncertainties of the present cross sections. The uncertainties due to limitations of the Landau-Zener model and the Fano-Lichten model are difficult to estimate. With some caution they may be assumed to be as large as 50%.

Figure 5 shows that the L-shell filling cross sections are seen to fluctuate around a typical value of ~ 10 a.u. This finding disagrees with the results adopted in our previous work [28], where the cross section was assumed to be proportional to the number of L-shell vacancies (and the proportionality constant was treated as a fitting parameter). Thus cross sections larger by a factor of ~ 5 were obtained for $n = 0$ (empty L shell) in comparison with the present results.

It should be recalled that the σ orbitals considered here cannot contain more than two vacancies. Hence the L-shell filling cross section is not expected to be proportional to the number of L-shell vacancies. Rather, as seen from Fig. 5, the cross sections σ_{Ln} vary in a nonmonotonic behavior. The values for $n = 0$ are relatively small, as already suggested by Grether et al. [24]. The maxima of the cross sections at intermediate n are produced by favorable curve-crossing mechanisms. It is noted also that the decrease of the cross section with decreasing projectile energy, previously observed [22,28], is confirmed by the present analysis. At the low-energy lim-

it of 0.135 keV the L-shell filling cross sections were found to be negligibly small. The disappearance of the collisional L-shell filling at very low projectile energies has also been anticipated [22], as the impact energy is not sufficient for the collision partners to reach the coupling radius R_c.

V. COMPARISON WITH EXPERIMENT

After determination of the cross sections for collisional L-shell filling, all the model parameters for the calculation of the transported intensities by Eqs. (6), (9), and (10) are known. We applied our calculations to the experimental results by Köhrbrück et al. [22] and Grether et al. [24], who measured L and K Auger electrons from hollow Ne atoms interacting with an Al surface. Particular attention was devoted to the attenuation of the Auger electrons in both the elastic and the inelastic channels.

It is noted that the experimental results are reported in arbitrary units so that the experiment was normalized to theory. In the following graphs, the units of the calculated intensities refer to the number of electrons ejected in all directions. This intensity, reduced by the solid angle, would reach the detector if the attenuation effects were negligible. Hence the maximum number of ejected K Auger electrons (summed over the L-shell occupation number) is equal to 1. This number may be as large as 8 for L Auger electrons. However, attenuation and side-feeding effects may cause significant reductions. To refer to a unit solid angle the data are to be divided by 4π.

Since the present results for the L-shell filling cross sections are quite different from those we have previously obtained [22,28], it is useful to analyze first the angular distributions of the K Auger electrons, which have extensively been studied in the past. As the K Auger electron emission from separated atoms is likely to be isotropic [48], the observation of anisotropic angular distributions may be attributed to absorption effects in the solid. Hence the angular distributions of the K Auger electrons provide direct evidence for attenuation effects [22].

To obtain the angular distributions, the K Auger intensities are summed over the L-shell occupation number n. In this case, details about the attenuations of Auger electrons for specific n values are lost. Therefore, we also focus our attention on examples of Auger intensities attributed to individual n values, which in turn govern the shape of the related Auger spectra.

A. Dependence on the observation angle

The results for the angular distributions are given in Fig. 6, where the Ne K Auger intensity is plotted as a function of the emission angle α relative to the Al surface plane. The experiments by Köhrbrück et al. [22] have been performed at projectile energies of 0.135, 1.0, 4.5, and 22.5 keV. As the travel distance l of the electrons in the solid is proportional to $1/\sin\alpha$, it is plausible that the attenuation increases with decreasing α. Also, it is plausible that the Auger emission depth, and hence the attenuation, increases as the projectile energy increases. The experimental data are compared with theoretical
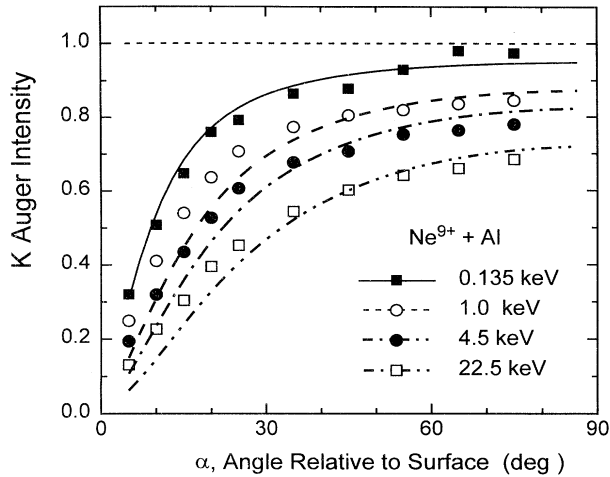
FIG. 6. Intensity of K Auger electrons ejected by Ne^{9+} impact on Al as a function of the angle α relative to the surface plane. The projectile energies are 0.135, 1.0, 4.5, and 22.5 keV as indicated. The experimental data are from Köhrbrück *et al.* [22]. The theoretical results are from Eq. (10) summed over the number n of L-shell electrons.

values for the total Auger intensity $Y_K = \sum_{n=2}^{8} Y_{Kn}$, obtained from Eq. (10) after summing over the number n of L-shell electrons. In Fig. 6 the agreement between the experimental data and the results from the model calculations is fairly good, except at small angles. This disagreement at glancing angles may be due to an enhanced excitation of surface plasmons [49].

It is noted that better agreement between experiment and theory is achieved when the L-shell filling cross sections are treated as adjustable fit parameters [22,28]. This finding is due to the tendency that the adjustments of fit parameters are likely to compensate for inaccuracies of other model parameters. In any case, it seems surprising that both the present model and that of Page *et al.* [28] reproduce the experimental data quite well since these models differ significantly in the L-shell filling cross sections. However, a closer inspection indicates that the differences in the cross sections and similar differences in the L Auger rates cancel each other partially in the calculations of the angular distributions. It is noted that such cancellations do not occur in the calculations of, e.g., the L Auger intensities.

Next we study K Auger intensities for individual numbers n of L-shell electrons. Figure 7 shows a bar diagram representing the transported intensities of K Auger electrons and their contributions from the elastic and the inelastic channels for different observation angles. When the electron observation angle is varied, the change of corresponding Auger intensities is uniquely produced by attenuation effects. It is seen that the Auger intensities for higher-n values are more reduced by attenuation effects. Moreover, as in Fig. 6, the 10° data are more affected than those observed at 50°. Consequently, the apparent mean value $\langle \tilde{n} \rangle_K$ of the L-shell occupation

number changes noticeably as the observation angle varies. The data in Fig. 7 show that this mean number increases from 3.9 to 4.5 as the observation angle changes from 10° to 50°. The change in $\langle \tilde{n} \rangle_K$ produces a shift of the centroid energy of the related Auger spectra. From the atomic-structure calculations by Schippers *et al.* [19] it is estimated that the present change of the L-shell occupation number and the production of inelastically scattered electrons correspond to a shift of the Auger spectra by ~ 8 eV.

In the past, the shift of the Auger spectra has been analyzed in terms of kinematic (Doppler) effects to determine the flight direction and the velocity of the projectile during the Auger emission [5,9,17,20]. This analysis is certainly sensitive on the energy shift of ~ 8 eV obtained here. For instance, Köhrbrück *et al.* [17] observed a shift of ~ 20 eV when changing the observation angle from $\alpha = 10°$ to 50° for 90-keV Ne^{9+} incident on Cu at an angle of $\psi = 10°$. (The perpendicular velocity for this projectile is approximately equal to that of the 4.5-keV Ne^{9+}
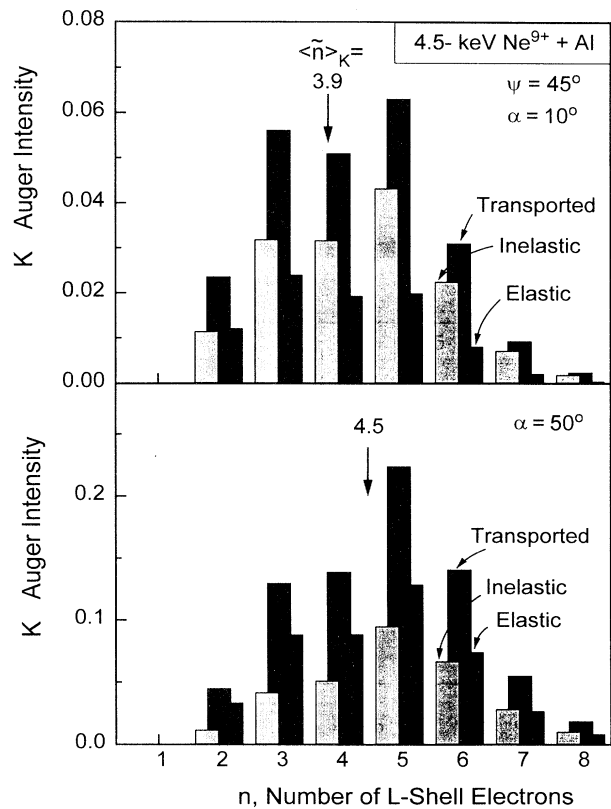

FIG. 7. Bar diagram for the intensities of transported K Auger electrons as a function of the number n of L-shell electrons. The transported intensities are the sum of the corresponding intensities in the elastic and inelastic channels. The projectile energy is 4.5 keV and the incidence angle is $\psi = 45°$. In the upper part, the electron observation angle is equal to $\alpha = 10°$ relative to the surface plane; in the lower part, $\alpha = 50°$. Note that the apparent mean number $\langle \tilde{n} \rangle_K$ of L-shell electrons is noticeably shifted as the observation angle is varied.

incident at 45°.) The energy shift has been attributed to a change of the flight direction of the projectile due to a specular deflection of the ions at the surface [17]. Further effects producing energy shifts of the Auger spectra have been discussed by Bleck-Neuhaus et al. [23]. It should be noted, however, that the previous studies deal primarily with energy shifts due to the buildup of inelastic intensity. The present analysis, which accounts for a variation of the attenuation with the L-shell occupation number n, provides also information about the energy shift of the elastic intensity. In view of the present results, care should be taken with regard to the possibility that a significant part of the Auger energy shift is due to attenuation effects. Further work is planned to analyze the apparent L-shell occupation number with varying observation angles.

B. Comparison of L and K Auger emission

To study attenuation effects for significantly different electron energies, we compare corresponding L and K Auger intensities as a function of the number n of L-shell electrons. From the analysis of the related Auger spectra, Grether et al. [24] have found that the mean numbers $\langle \bar{n} \rangle_L$ and $\langle \bar{n} \rangle_K$ attributed to L and K Auger transitions, respectively, are quite different. As shown in Table II, the experimental results are $\langle \bar{n} \rangle_L^{expt}=2$ and $\langle \bar{n} \rangle_K^{expt}=4.5$. Due to differences in the related Auger transition rates we would expect differences in these mean values. However, in view of the foregoing analysis, it is interesting to verify also the role of attenuation effects.

Figure 8 shows the analysis of the L and K Auger intensities by means of a bar diagram. The hatched bars, labeled *ejected*, represent the intensity of the Auger electrons emitted in all directions from the hollow Ne atom as a function of the L-shell occupation number n. It should be recalled that this intensity (reduced by the detector solid angle) would reach the detector if the attenuation of the electrons were negligible in the solid. The corresponding attenuated intensities are represented by the solid bars labeled *transported*. It should also be recalled that the ejected and the transported intensities were obtained by means of Eq. (10) with $\Gamma_K^a=0$ and $\Gamma_K^a\neq0$, respectively.

From Fig. 8 it is seen that the attenuation effects become dominant for larger values of n. As expected, the attenuation increases with increasing number of L-shell electrons, as the corresponding Auger electrons are ejected from a larger depth. It is also noted that the L Auger electrons are by far more affected by attenuation than the K Auger electrons. This is due to the fact that the attenuation length for the ~100-eV L-shell Auger electrons is significantly smaller than that for the ~780-eV K-shell Auger electrons (Table I). In addition, Fig. 9 provides more detailed information about the transport mechanisms of the Auger electrons. The bar diagrams show the contributions of the elastic and the inelastic channels to the transported intensities. It is seen that the inelastic contribution increases strongly with respect to the elastic contribution as the L-shell occupation number n increases. Again this is understood from the deeper emission of the Auger electron for high-n values.
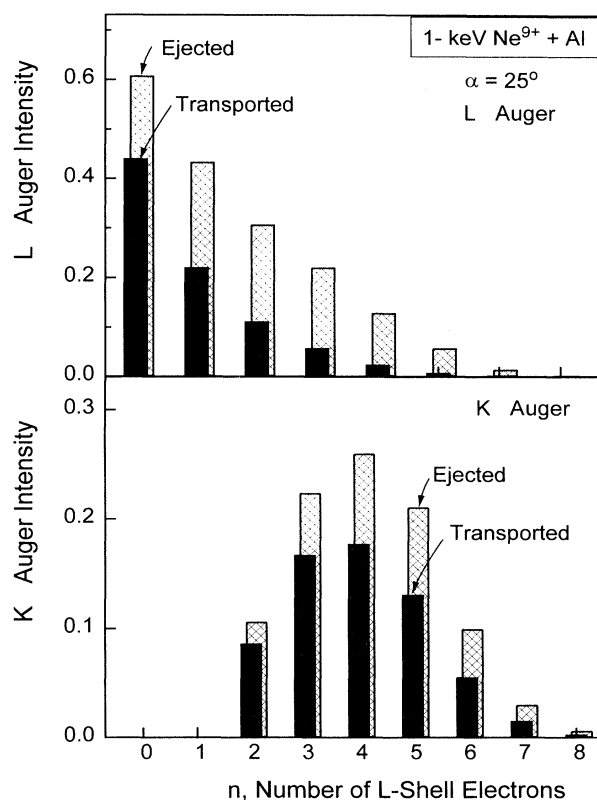
The significant attenuation creates noticeable

FIG. 8. Bar diagram for the intensities of ejected and transported L and K Auger electrons as a function of the number n of L-shell electrons. The projectile energy is 1 keV, the incidence angle is equal to $\psi=45°$, and the electron observation angle is equal to $\alpha=25°$ relative to the surface plane. The hatched bars represent the electrons ejected by the hollow Ne atoms. The solid bars represent the transported electrons that reach the detector after attenuation in the solid. Note that the transported intensities include both the elastic and the inelastic channels.

TABLE II. Mean L-shell occupation number during the L and the K Auger transitions produced by 1-keV Ne^{9+} impact on Al. The real and the apparent values are evaluated from Eq. (12) with zero and nonzero attenuation of the Auger electrons, respectively. The experimental results are taken from Grether et al. [24].

	Transition	
Type	L Auger	K Auger
Real	$\langle n \rangle_L=1.5$	$\langle n \rangle_K=4.1$
Apparent	$\langle \bar{n} \rangle_L=0.9$	$\langle \bar{n} \rangle_K=3.8$
Experimental	$\langle \bar{n} \rangle_L^{expt}=2\pm1$	$\langle \bar{n} \rangle_K^{expt}=4.5\pm1$

N. STOLTERFOHT *et al.*

differences in the real and the apparent number of L-shell electrons evaluated by means of Eq. (12) with zero and nonzero attenuation, respectively. The results for 1-keV Ne^{9+} impact are shown in Table II in comparison with the experimental data. It is seen for K Auger emission that the mean numbers $\langle n \rangle_K$ and $\langle \bar{n} \rangle_K$ differ by about 8%. However, this difference increases significantly for L Auger emission, i.e., $\langle n \rangle_L$ and $\langle \bar{n} \rangle_L$ differ by about 60%. Hence it is evident that attenuation effects are to be taken into account when these results are compared with the experimental data.

It is found, however, that the experimental data by Grether *et al.* [24] agree better with the actual mean values than with the apparent mean values (Table II). In regard to relative large experimental uncertainties of about ±1, this agreement is considered to be accidental. It is more important to keep in mind that the model calculations are capable of reproducing the significant difference between the mean L-shell occupation numbers observed in the L and the K Auger spectra. This indicates that the basic features of the dynamics for filling the

FIG. 9. Bar diagram for the intensities of transported L and K Auger electrons as a function of the number n of L-shell electrons as in Fig. 8. The transported intensities are the sum of the corresponding intensities in the elastic and the inelastic channels. Note that the intensity in the inelastic channel increases in comparison with that in the elastic channel as the number of L-shell electrons increases.

L and the K shell are adequately described by the present model.

To understand the difference in the experimental mean values $\langle \bar{n} \rangle_L^{expt}$ and $\langle \bar{n} \rangle_K^{expt}$ for L and K Auger emission, respectively, we focus our attention on the data in Table I that exhibit the essential features of the L and K Auger transitions. The L Auger rates are dominant for the empty L shell and the related collisional filling cross sections are relatively small so that the L Auger intensities maximize at $n = 0$ (Figs. 8 and 9). On the other hand, the K Auger rates are equal to zero for $n = 0$ and 1 and they maximize at high n (Fig. 3). Therefore, it is plausible that the K Auger intensity has a maximum at higher n. These considerations show that the difference in the mean occupations number observed for L and K Auger emission is primarily produced by the differences in the competing filling mechanisms.

VI. DISCUSSION AND CONCLUSIONS

A multiple cascade model is used to study detailed aspects associated with the filling of hollow Ne atoms moving below the surface. For projectile energies larger than ~ 1 keV we expect that above-surface Auger emission can be neglected. The present model, which is based on the previous analysis by Page *et al.* [28], exhibits various characteristic features. It assumes a straight-line trajectory for the incident ion in the solid and hence it applies for sufficiently high energies at which the projectile-solid scattering is small. On the other hand, absorption and buildup effects on the ejected electrons are incorporated in a manner such that analytic solutions are retained for the integrated Auger intensities. Therefore, the present model provides an efficient tool to study effects produced by the attenuations of electrons moving below the surface.

Emphasis is given to the *a priori* determination of a complete set of model parameters responsible for the competing mechanisms filling the projectile in the solid. Cross sections for collisional L-shell filling of hollow projectile atoms are evaluated. The analysis is based on molecular-orbital calculations that account for properties of hollow atoms. Furthermore, solid-state effects are included in the derivation of the asymptotic orbital energies. The capture processes are described by simple models including mechanisms of curve crossing and orbital promotion. Curve crossings are often a result of a strong orbital demotion that was shown to be a characteristic feature of hollow atoms. Also, the $4f\sigma$ orbital promotion is evaluated in the solid involving efficient vacancy transfer from deeply lying levels into the conduction band.

It is pointed out that notable uncertainties for the L-shell filling cross sections result from the limitations of the Landau-Zener and the Fano-Lichten models. These simple models, however, are felt to be justified for the present case where the charge transfer into hollow atoms is calculated. We expect that the present research of hollow atoms will motivate further studies involving improved theoretical methods. Nevertheless, remarkable gross features can be extracted from the present model
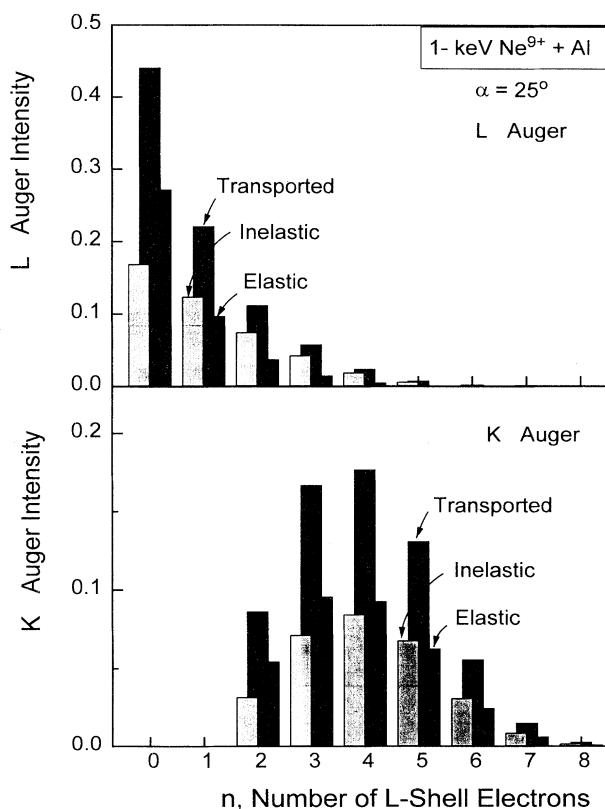
calculations. For instance, it is safe to conclude that the L-shell filling cross sections maximize at intermediate occupation numbers determined by favorable curve-crossing mechanisms. Thus it is not possible for the cross sections to be proportional to the number of L-shell vacancies.

Additional effort is devoted to the reliable determination of the other model parameters, such as the attenuation lengths of the electrons in the solid and the K Auger rates. In the set of model parameters, the remaining uncertainty refers to the evaluation of the L Auger rates. In this case, rough estimates are made on the basis of Auger rates for separated atoms. Future work is planned to determine the L Auger rates by means of localized solid-state wave functions. Also, the missing L Auger channels, opened after the K Auger transition, shall be implemented.

Experimental data for angular distributions of the K Auger electrons agree fairly well with the present cascade model. Better agreement was obtained from our previous fitting procedures [22,28]. It should be realized, however, that this good agreement often holds only for the case in which the model parameters are optimized. The present *a priori* evaluation of the model parameters is expected to yield reasonable agreement in more general cases, concerning various phenomena of hollow atoms. Hence a detailed understanding may be achieved for these unusual atomic species.

The comparison with experimental data is primarily devoted to individual L-shell occupation numbers and the alteration of the corresponding Auger intensities by attenuation effects. Since considerable attenuation of the electrons is observed, it useful to distinguish between apparent and actual mean values in the description of hollow atoms. For instance, the Auger decay of projectiles with increasing L-shell occupation takes place in deeper layers so that the attenuation becomes more important. Therefore, the high-energy part of the Auger spectra, associated with high-L shell occupation numbers, is more reduced than the low-energy part. As a consequence, the Auger spectra are subject to energy shifts that may conflict with related kinematic shifts. Also, it follows that the apparent L-shell occupation number is smaller than the actual mean number.

Finally, the present cascade model is applied to verify the previous observation of a significant difference appearing in the L-shell occupation numbers during L and K Auger emission. As before, attenuation effects are found to be significant; however, they are insufficient to explain the observed differences in the mean occupation numbers. In this case, it is shown that differences in the L- and the K-shell filling rates are responsible for the experimental observation. The present analysis indicates that L Auger transitions take place much closer to the surface than the corresponding K Auger transitions. Hence the L and the K Auger electrons can be used as tools for probing different regions near the surface. Future work is planned to intensify the comparison of L and K Auger emission from hollow atoms.

ACKNOWLEDGMENTS

[1] U. A. Arifov, E. S. Mukhamadiev, E. S. Parilis, and A. S. Pasyuk, Zh. Tekh. Fiz. **43**, 375 (1973) [Sov. Phys. Tech. Phys. **18**, 240 (1973)].

[2] E. D. Donets, Nucl. Instrum. Methods Phys. Res. Sect. B **9**, 522 (1985).

[3] D. M. Zehner, S. H. Overbury, C. C. Havener, F. W. Meyer, and W. Heiland, Surf. Sci. **178**, 359 (1986).

[4] F. W. Meyer, C. C. Havener, S. H. Overbury, K. J. Snowdon, D. M. Zehner, W. Heiland, and H. Hemme, Nucl. Instrum. Methods Phys. Res. Sect. B **23**, 234 (1987); F. W. Meyer, C. C. Havener, K. J. Snowdon, S. H. Overbury, D. M. Zehner, and W. Heiland, Phys. Rev. A **35**, 3176 (1987).

[5] S. T. de Zwart, A. G. Drentje, A. L. Boers, and R. Morgenstern, Surf. Sci. **217**, 298 (1989).

[6] H. J. Andrä, Nucl. Instrum. Methods Phys. Res. Sect. B **43**, 306 (1989).

[7] P. Varga, Comments At. Mol. Phys. **23**, 111 (1989).

[8] J. P. Briand, L. de Billy, P. Charles, S. Essabaa, P. Briand, R. Geller, J. P. Desclaux, S. Bliman, and C. Ristori, Phys. Rev. Lett. **65**, 159 (1990); J. P. Briand, L. de Billy, P. Charles, J. P. Desclaux, P. Briand, R. Geller, S. Bliman, and C. Ristori, Europhys. Lett. **15**, 233 (1991); Z. Phys. D

21, S123 (1991).

[9] L. Folkerts and R. Morgenstern, Europhys. Lett. **13**, 377 (1990); Z. Phys. D **21**, S351 (1991).

[10] F. Aumayr, G. Lakits, and HP. Winter, Appl. Surf. Sci. **47**, 139 (1991); H. Kurz, K. Töglhofer, HP. Winter, and F. Aumayr, Phys. Rev. Lett. **69**, 1140 (1992); F. Aumayr and HP. Winter, Comments At. Mol. Phys. **29**, 275 (1994).

[11] H. Winter, Europhys. Lett. **18**, 207 (1992); H. Winter, C. Auth, R. Schuch, and E. Beebe, Phys. Rev. Lett. **71**, 1939 (1993).

[12] U. Wille, Nucl. Instrum. Methods Phys. Res. Sect. B **67**, 132 (1992); Phys. Rev. A **45**, 3004 (1992).

[13] J. McDonald, D. Schneider, M. Clark, and D. Dewitt, Phys. Rev. Lett. **68**, 2297 (1992).

[14] J. Burgdörfer, in *Review of Fundamental Processes and Applications of Atoms and Ions,* edited by C. D. Lin (World Scientific, Singapore, 1993), p. 517.

[15] F. W. Meyer, S. H. Overbury, C. C. Havener, P. A. Zeijlmans van Emmichoven, and D. M. Zehner, Phys. Rev. Lett. **67**, 723 (1991); F. W. Meyer, S. H. Overbury, C. C. Havener, P. A. Zeijlmans van Emmichoven, J. Burgdörfer, and D. M. Zehner, Phys. Rev. A **44**, 7214 (1991).

[16] J. Burgdörfer, P. Lerner, and F. W. Meyer, Phys. Rev. A **44**, 5674 (1991); J. Burgdörfer and F. W. Meyer, *ibid.* **47**, R20 (1993).

[17] R. Köhrbrück, D. Lecler, F. Fremont, P. Roncin, K. Sommer, T. J. M. Zouros, J. Bleck-Neuhaus, and N. Stolterfoht, Nucl. Instrum. Methods Phys. Res. Sect. B **56/57**, 219 (1991); R. Köhrbrück, K. Sommer, J. P. Biersack, J. Bleck-Neuhaus, S. Schippers, P. Roncin, D. Lecler, F. Fremont, and N. Stolterfoht, Phys. Rev. A **45**, 4653 (1992).

[18] H. J. Andrä, A. Simionovici, T. Lamy, A. Brenac, G. Lamboley, J. J. Bonnet, A. Fleury, M. Bonnefoy, M. Chassevent, S. Andriamonje, and A. Pesnelle, Z. Phys. D **21**, S301 (1991); H. J. Andrä, A. Simionivici, T. Lamy, A. Brenac, and A. Pesnelle, Europhys. Lett. **23**, 361 (1993).

[19] S. Schippers, S. Hustedt, W. Heiland, R. Köhrbrück, J. Kemmler, D. Lecler, J. Bleck-Neuhaus, and N. Stolterfoht, Phys. Rev. A **46**, 4003 (1992); S. Schippers, S. Hustedt, W. Heiland, R. Köhrbrück, J. Bleck-Neuhaus, J. Kemmler, D. Lecler, and N. Stolterfoht, Nucl. Instrum. Methods Phys. Res. Sect. B **78**, 106 (1993).

[20] J. Das, L. Folkerts, and R. Morgenstern, Phys. Rev. A **45**, 4669 (1992); J. Das and R. Morgenstern, *ibid.* **47**, R755 (1993).

[21] J. Limburg, J. Das, S. Schippers, R. Hoekstra, and R. Morgenstern, Surf. Sci. **313**, 355 (1994).

[22] R. Köhrbrück, M. Grether, A. Spieler, N. Stolterfoht, R. Page, A. Saal, and J. Bleck-Neuhaus, Phys. Rev. A **50**, 1429 (1994).

[23] J. Bleck-Neuhaus, A. Saal, R. Page, P. Biermann, R. Köhrbrück, and N. Stolterfoht, Phys. Rev. A **49**, R1529 (1994).

[24] M. Grether, A. Spieler, R. Köhrbrück, and N. Stolterfoht, Phys. Rev. A (to be published).

[25] S. Schippers, J. Limburg, J. Das, R. Hoekstra, and R. Morgenstern, Phys. Rev. A **50**, 540 (1994).

[26] P. M. Echenique, F. Flores, and R. H. Ritchie, in *Solid State Physics: Advances in Research and Applications,* edited by H. Ehrenreich and D. Turnbull (Academic, New York, 1990), Vol. 43, p. 230.

[27] J. Burgdörfer, C. Reinhold, and F. W. Meyer, Nucl. Instrum. Methods Phys. Res. Sect. B (to be published).

[28] R. Page, A. Saal, J. Thomaschewski, J. Bleck-Neuhaus, R. Köhrbrück, M. Grether, and N. Stolterfoht, Phys. Rev. A (to be published).

[29] C. D. Landau, J. Phys. (Moscow) **2**, 46 (1932); C. Zener, Proc. R. Soc. London Ser. A **137**, 696 (1932).

[30] U. Fano and W. Lichten, Phys. Rev. Lett. **14**, 627 (1965).

[31] N. Stolterfoht, R. Köhrbrück, M. Grether, A. Spieler, A. Arnau, R. Page, A. Saal, J. Thomaschewski, and J. Bleck-Neuhaus, International Conference on the Use of Accelerators in Industry and Research, Denton, 1994 [Nucl. Instrum. Methods Phys. Res. Sect. B (to be published)].

[32] E. Segré, *Nuclei and Particles* (Benjamin, New York, 1964).

[33] H. Limburg, S. Schippers, I. Hughes, R. Hoekstra, R. Morgenstern, S. Hustedt, N. Hatke, and W. Heiland, Phys. Rev. A **51**, 3873 (1995).

[34] S. Hustedt, J. Freese, S. Mähl, W. Heiland, S. Schippers, J. Bleck-Neuhaus, M. Grether, R. Köhrbrück, and N. Stolterfoht, Phys. Rev. A **50**, 4993 (1994).

[35] R. Köhrbrück, N. Stolterfoht, S. Schippers, S. Hustedt, W. Heiland, D. Lecler, J. Kemmler, and J. Bleck-Neuhaus, Phys. Rev. A **48**, 3731 (1993).

[36] M. H. Chen and B. Craseman, Phys. Rev. A **12**, 959 (1975).

[37] M. O. Krause, J. Phys. Chem. Ref. Data **8**, 307 (1979).

[38] R. Nunez, P. M. Echenique, and R. H. Ritchie, J. Phys. C **13**, 4229 (1980).

[39] A. Arnau, R. Köhrbrück, M. Grether, A. Spieler, and N. Stolterfoht, Phys. Rev. A **51**, 3399 (1995).

[40] N. Stolterfoht, in *Progress in Atomic Spectroscopy,* edited by H. Kleinoppen (Plenum, New York, 1987), Pt. D, p. 415.

[41] E. Zaremba, L. M. Sander, H. B. Shore, and J. H. Rose, J. Phys. F **7**, 1763 (1977).

[42] A. Arnau, P. A. Zeijlmans, J. I. Juaristi, and E. Zaremba, Nucl. Instrum. Methods Phys. Res. Sect. B (to be published).

[43] The present analysis including the numerical diagonalization was performed using the symbolic mathematics code by S. Wolfram, *Mathematica: A System for Doing Mathematics by Computers,* 2nd ed. (Addison-Wesley, Redwood City, CA, 1991).

[44] M. Barat and W. Lichten, Phys. Rev. A **6**, 211 (1972).

[45] R. K. Cacak, Q. C. Kessel, and M. E. Rudd, Phys. Rev. A **2**, 1327 (1970); Q. C. Kessel, Bull. Am. Phys. Soc. **14**, 946 (1966).

[46] Yu. N. Demkov, Zh. Eksp. Teor. Fiz. **45**, 195 (1963) [Sov. Phys. JETP **18**, 138 (1964)].

[47] E. E. Nikitin, Opt. Spektrosk. **13**, 761 (1962) [Opt. Spectrosc. (USSR) **13**, 431 (1962)].

[48] N. Stolterfoht, Phys. Rep. **146**, 315 (1987).

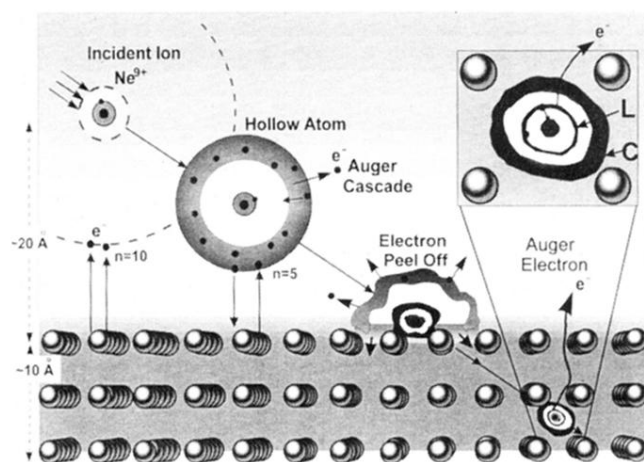[49] P. M. Echenique and J. P. Pendry, J. Phys. C **8**, 2936 (1975).

FIG. 1. Formation of hollow atoms above and below the surface. At distances of about 20 Å, the incident Ne^{9+} ion captures several electrons into the Rydberg state $n = \sim 10$. These "large" hollow atoms undergo an Auger cascade reaching lower Rydberg states, e.g., $n = 5$. When the atom hits the surface it is still hollow and the Rydberg electrons are removed (electron peel-off). Simultaneously a dynamic screening cloud (labeled C) is formed around the ion, whereas the L shell (labeled L) stays empty for a certain time. Thus, as shown in the inset, a "small" hollow atom is formed in the solid.
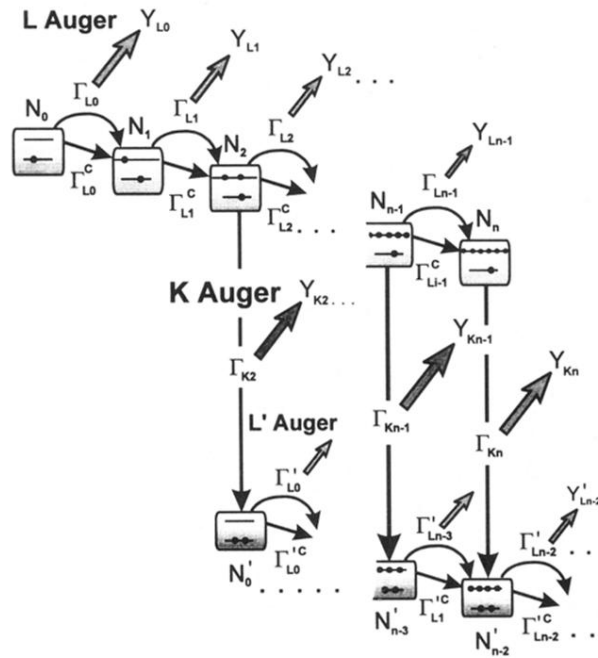
FIG. 2. Diagram for multiple cascade processes in hollow atoms moving below a surface. The label n specifies the number of L-shell electrons. The quantities Γ_{Ln} and Γ_{Kn} are L and K Auger rates. The quantities Γ_{Ln}^c are rates for collisional transfer of an electron into the L shell. The arrows indicate the intensity of the ejected L and K Auger electrons.
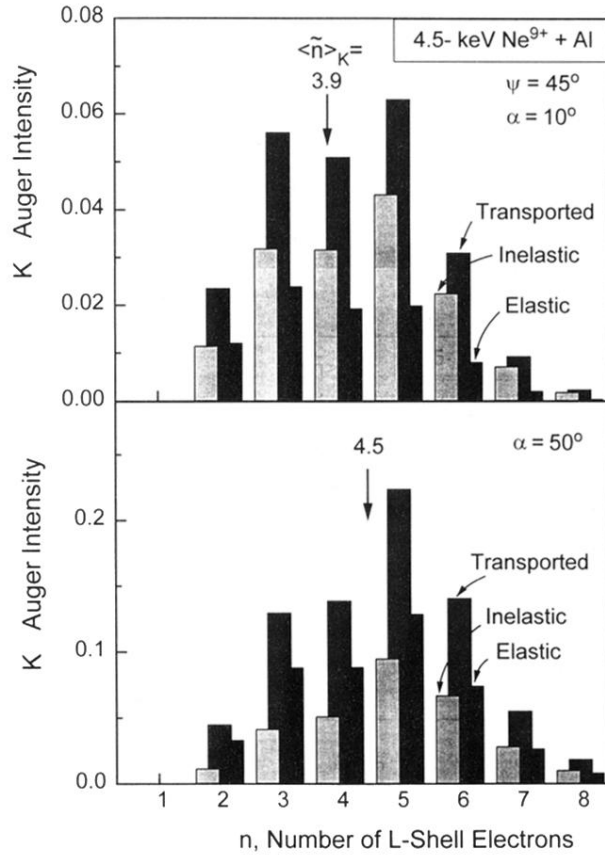
FIG. 7. Bar diagram for the intensities of transported K Auger electrons as a function of the number n of L-shell electrons. The transported intensities are the sum of the corresponding intensities in the elastic and inelastic channels. The projectile energy is 4.5 keV and the incidence angle is $\psi = 45°$. In the upper part, the electron observation angle is equal to $\alpha = 10°$ relative to the surface plane; in the lower part, $\alpha = 50°$. Note that the apparent mean number $\langle \tilde{n} \rangle_K$ of L-shell electrons is noticeably shifted as the observation angle is varied.
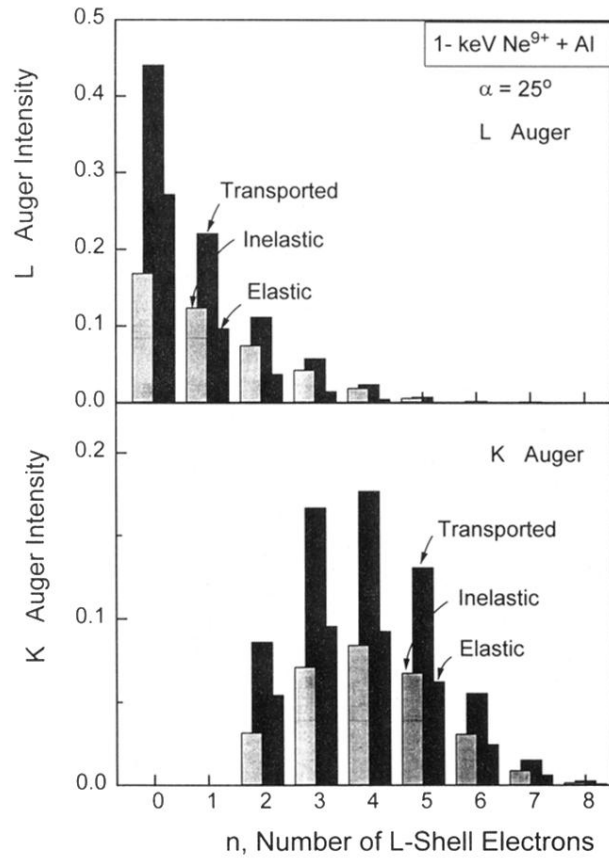
FIG. 9. Bar diagram for the intensities of transported L and K Auger electrons as a function of the number n of L-shell electrons as in Fig. 8. The transported intensities are the sum of the corresponding intensities in the elastic and the inelastic channels. Note that the intensity in the inelastic channel increases in comparison with that in the elastic channel as the number of L-shell electrons increases.